JOURNAL OF AIRCRAFT
Vol. 37, No. 4, July–August 2000

# Modeling Human Pilot Cue Utilization with Applications to Simulator Fidelity Assessment

Y. Zeyada* and R. A. Hess†
*University of California, Davis, Davis, California 95616*

**An analytical investigation to model the manner in which pilots perceive and utilize visual, proprioceptive, and vestibular cues in a ground-based flight simulator was undertaken. Data from a NASA Ames Research Center vertical motion simulator study of a simple, single-degree-of-freedom rotorcraft bob-up/down maneuver were employed in the investigation. The study was part of a larger research effort that has the creation of a methodology for determining flight simulator fidelity requirements as its ultimate goal. The study utilized a closed-loop feedback structure of the pilot/simulator system that included the pilot, the cockpit inceptor, the dynamics of the simulated vehicle, and the motion system. With the exception of time delays that accrued in visual scene production in the simulator, visual scene effects were not included in this study. Pilot/vehicle analysis and fuzzy-inference identification were employed to study the changes in fidelity that occurred as the characteristics of the motion system were varied over five configurations. The data from three of the five pilots who participated in the experimental study were analyzed in the fuzzy-inference identification. Results indicate that both the analytical pilot/vehicle analysis and the fuzzy-inference identification can be used to identify changes in simulator fidelity for the task examined.**

## Nomenclature

$\boldsymbol{A}, \boldsymbol{B}$ = matrices in state-space description of vehicle dynamics
$C$ = input to structural pilot model
$E$ = error signal in structural pilot model
$E_M$ = input to closed neuromuscular/vestibular control loop in structural pilot model
$h, \dot{h}, \ddot{h}$ = height deviation, velocity, and acceleration in bob-up/down maneuver, ft, ft/s, ft/s$^2$
$h_c$ = input to modeled pilot/vehicle system, ft
$h_{\text{com}}$ = inverse dynamics command to modeled pilot/vehicle system, ft
$h_{\text{des}}$ = desired vertical position time history for modeled pilot/vehicle, ft
$\ddot{h}_{\text{motion}}/\ddot{h}_{\text{command}}$ = simulator motion dynamics
$K_e$, $K_{\dot{m}}$ = gain values in visual and vestibular loops in structural pilot model
$K_h$ = gain in pilot transfer function $Y_{p_h}$
$T_d$ = completion time in bob-up/down maneuver, used in defining $h_{\text{des}}$, s
$U_M$ = proprioceptive feedback variable in structural pilot model
$U_S$ = vestibular feedback variable in structural pilot model
$\boldsymbol{u}$ = control vector in state-space description of vehicle dynamics
$V_{\text{BU}}$, $V_{\text{BD}}$ = volumes beneath fuzzy inference surface view plots for bob-up (BU) and bob-down (BD) maneuvers
$\boldsymbol{x}$ = state-variable matrix in state-space description of vehicle dynamics
$Y_C$ = transfer function of vehicle in structural pilot model
$Y_{\text{FS}}$ = transfer function of force-feel system in structural pilot model
$Y_{\text{NM}}$ = transfer function of neuromuscular system in structural pilot model
$Y_P$ = transfer function of structural pilot model, $(M/C)$
$Y_{p_h}$ = transfer function of pilot model for outer, position loop in bob-up/down task
$z$ = dynamic inflow variable in state-space description of vehicle dynamics, ft/s$^2$
$\delta_c$ = collective inceptor motion, in.
$\delta_M$ = structural pilot model output, identical to $\delta_c$
$\zeta_{\text{NM}}$ = damping ratio in transfer function of neuromuscular system in structural pilot model
$\tau_0$ = time delay in structural pilot model, s
$\omega_c$ = crossover frequency, rad/s
$\omega_{\text{NM}}$ = undamped natural frequency in transfer function of neuromuscular system in structural pilot model, rad/s

Received 6 October 1999; revision received 15 March 2000; accepted for publication 5 April 2000. 

*Postgraduate Researcher, Department of Mechanical and Aeronautical Engineering, One Shields Avenue.
†Professor and Vice Chairman, Department of Mechanical and Aeronautical Engineering. Associate Fellow AIAA.

## Introduction and Background

VALIDATING the fidelity of ground-based flight simulators is a problem of continuing interest to the simulation community. The ultimate objective of the research to be described is the development of a procedure for determining simulation requirements that will ensure acceptable fidelity. The need for such requirements can be clearly seen from Fig. 1, taken from Ref. 1. Here a comparison is made between the Cooper–Harper pilot opinion ratings obtained from flight-test and moving-base simulator evaluations for a group of low-speed rotorcraft maneuvers. As Fig. 1 indicates, there exists a significant difference between the ratings given in flight and simulation, indicating shortcomings in the fidelity of the simulator. An analytical approach to addressing some of these problems was discussed by Hess et al.[2,3]

The approach to be discussed builds on the work of Refs. 2 and 3 and utilizes a model of the pilot's perceptual and response characteristics as captured in the structural pilot model discussed by Hess.[4] In addition, fuzzy-inference identification of human pilot behavior is exploited. Although the use of fuzzy-inference models to describe human control behavior is not new, to the authors' knowledge this is the first time they have been employed in simulator fidelity studies.[5,6]

## Experiment

A pilot-in-the-loop simulation of a rotorcraft bob-up/down maneuver using the NASA Ames Research Center vertical motion simulator (VMS) provides the database for the study. Details of this simulation can be found in Ref. 7. A simplified rotorcraft model

**Table 1 Motion configurations**

| Configuration | $\ddot{h}_{\text{motion}}/\ddot{h}_{\text{command}}$ |
|---|---|
| V1 | 1.0 |
| V10 | 0 |
| V13 | 0.5 |
| V14 | $\dfrac{0.5s^2}{s^2 + 2(0.707)0.521s + 0.521^2}$ |
| V15 | $\dfrac{0.5s^2}{s^2 + 2(0.707)0.885s + 0.885^2}$ |

**Table 2 Task performance standards**

| Segment | Desired | Adequate |
|---|---|---|
| Ascent, s | <6 | <10 |
| 10 s at top, ft | ±2 | ±5 |
| Descent, s | <6 | <10 |
| 10 s at bottom, ft | ±2 | ±5 |

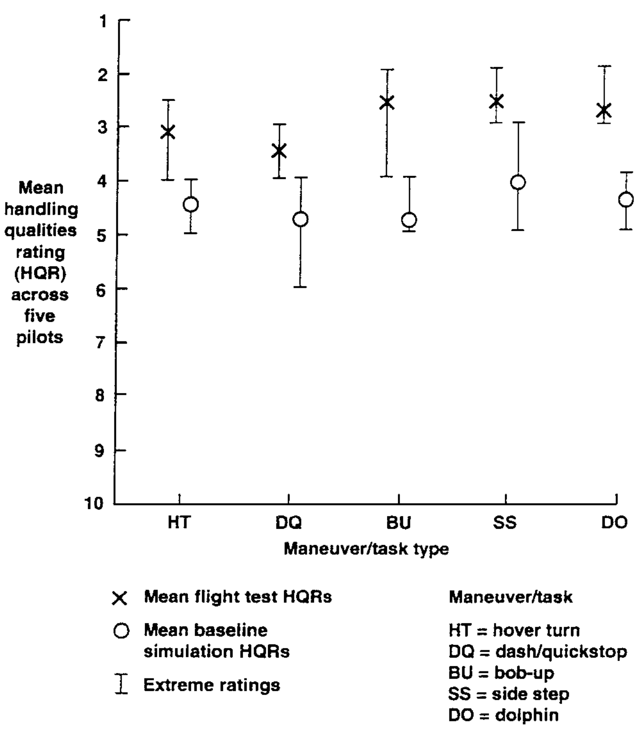


**Fig. 1 Differences between in-flight and simulator evaluations from Ref. 1.**

was employed in the simulation study with the characteristics of the motion and visual systems serving as the experimental variables. The vehicle dynamics are

$$\dot{\boldsymbol{x}}(t) = \boldsymbol{A}\boldsymbol{x}(t) + \boldsymbol{B}\boldsymbol{u}(t)$$

$$\boldsymbol{A} = \begin{bmatrix} -0.122 & -118 \\ 0 & -12.9 \end{bmatrix} \qquad \boldsymbol{B} = \begin{bmatrix} 14.6 \\ 1 \end{bmatrix}$$

$$\boldsymbol{x}(t) = [\dot{h}(t) \quad z(t)]^T \qquad \boldsymbol{u}(t) = \delta_C(t - 0.15)$$

An additional 0.12-s time delay was included in visual and motion channels in the pilot/vehicle analysis to account for VMS delays.[7] Table 1 describes the subset of the motion system dynamics investigated herein. The task consisted of a bob-up from a stabilized hover to a target 32 ft above the initial rotorcraft position, a stabilized hover, then a bob-down to the original position. Figure 2 is a representation of the geometry of the task. The visual cues available to the pilots were identical in all of the tasks analyzed. Constraints were placed on the translation time to ensure aggressive pilot behavior. Task performance standards are given in Table 2. Five pilots were used in the experiment and the data from the first three of the pilots involved in the simulation were analyzed here. The choice of pilots whose data were to be analyzed was arbitrary, and limiting the number to three was done for convenience. Each of the three pilots whose data were analyzed were NASA test pilots. For the purposes of this study, the important experimental results were the subjective pilot Cooper–Harper handling qualities ratings (HQRs), pilot-induced oscillation ratings (PIORs) and motion fidelity ratings (MFRs).[7] The scales describing these ratings are shown in Figs. 3 and 4 and Table 3. The pilot-induced oscillation (PIO) scale of Fig. 4 is taken from Ref. 8. Table 4 summarizes the pilot rating data for the three pilots whose data were analyzed in this study. The average composite score shown in Table 4 was an attempt to obtain an average numerical score reflecting the HQR, PIOR, and MFR for all three pilots (A, B, and C). The score was calculated as follows:

**Table 3 Motion fidelity scale from Ref. 7**

| Fidelity rating | Definition | Numerical rating[a] |
|---|---|---|
| High | Motion sensations like those of flight | 3 |
| Medium | Motion sensations are noticeably different from flight, but not objectionable | 2 |
| Low | Motion sensations are noticeably different from flight and objectionable | 1 |

[a]Numerical rating assigned for purposes of analysis.

**Table 4 Pilot rating and fuzzy inference identification summary**

| | Pilot | | | Average | Average |
|---|---|---|---|---|---|
| Configuration | A, B, C HQR | A, B, C PIOR | A, B, C MFR | composite score | normalized SVM |
| V1 | 3, 2, 3 | 1, 1, 2 | 2, 3, 2 | 1.00 | 1.0 |
| V10 | 5, 4, 4 | 5, 3, 3 | 1, 1, 1 | 2.19 | 2.27 |
| V13 | 4, 3, 2 | 4, 2, 2 | 2, 3, 3 | 1.21 | 1.28 |
| V14 | 5, 5, 4 | 4, 3, 4 | 2, 2, 2 | 1.69 | 2.39 |
| V15 | 4, 4, 3 | 2, 2, 3 | 2, 3, 2 | 1.28 | 2.09 |
| Nominal | 3, 3, 3[a] | 2, 2, 2[a] | ∞, ∞, ∞[b] | 0.54 | —— |

[a]Nominal vehicle HQRs and PIORs estimated from structural model results.
[b]Nominal vehicle given an MFR of ∞, that is, last terms in numerator and denominator of Eq. (1) are zero.

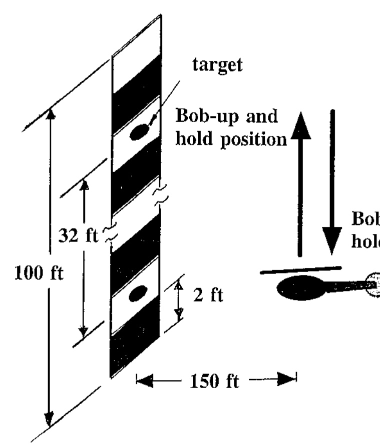


**Fig. 2 NASA VMS task geometry.**

$$\text{average composite score, configuration } j = \left[\sum_{i=1}^{3}(\text{HQR}_i)_j + \sum_{i=1}^{3}(\text{PIOR}_i)_j \cdot \frac{10}{6} + \sum_{1}^{3}\frac{1}{(\text{MFR}_i)_j}\cdot 10\right] \Bigg/ \min_{\text{all } j}\left[\sum_{i=1}^{3}(\text{HQR}_i)_j + \sum_{i=1}^{3}(\text{PIOR}_i)_j \cdot \frac{10}{6} + \sum_{1}^{3}\frac{1}{(\text{MFR}_i)_j}\cdot 10\right] \tag{1}$$

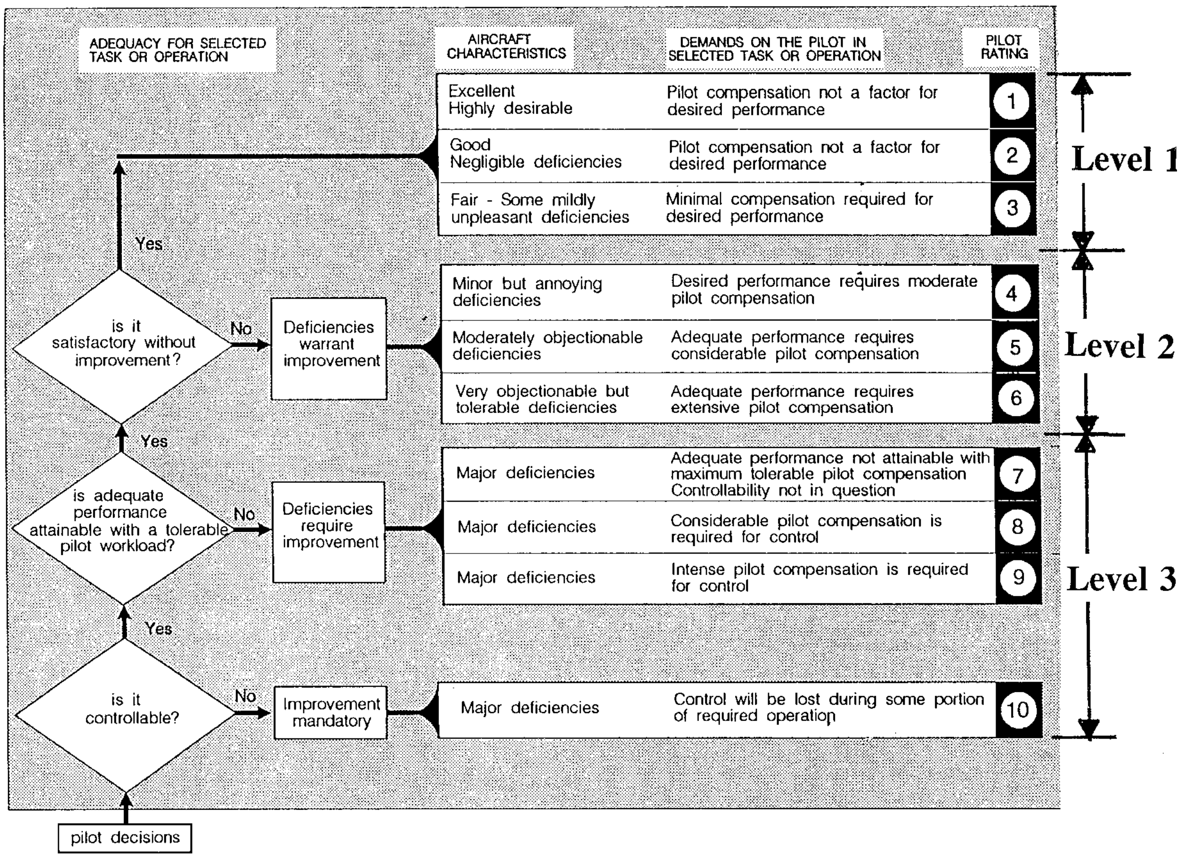


**Fig. 3 Cooper–Harper rating scale.**

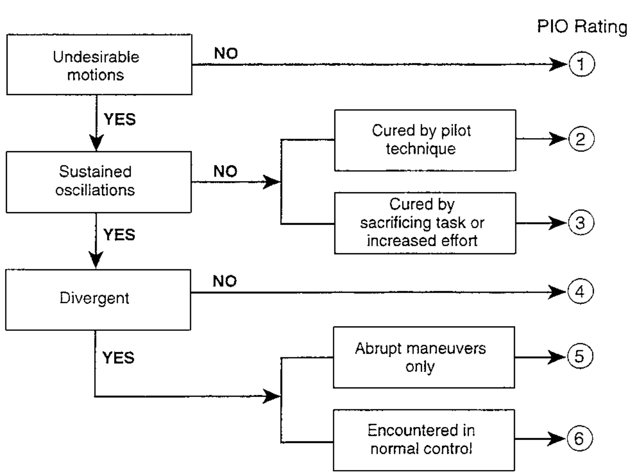


**Fig. 4 PIO rating scale.**

where $(\mathrm{HQR}_i)_j$ is the numerical HQR given by the $i$th pilot for the $j$th configuration, $(\mathrm{PIOR}_i)_j$ is the numerical PIOR given by the $i$th pilot for the $j$th configuration, and $(\mathrm{MFR}_i)_j$ is the numerical MFR for the $i$th pilot for the $j$th configuration.

In Eq. (1), $j$ represents one of the five motion system configurations, V1, V10, V13, V14, and V15, in Table 1. The denominator of Eq. (1) represents the best system as reflected in the weighted sum of the three ratings assigned by the pilots. Note that, in Table 1, configurations V1–V15 are merely ordered numerically, that is, the order does not reflect a presumed ranking of fidelity. The factors $\frac{10}{6}$ and 10 applied to the PIOR and 1/MFR ratings means that the worst Cooper–Harper rating, worst PIO rating, and worst fidelity rating would make equal contributions of 10 to the numerator of Eq. (1). In contrast, the best ratings would make respective contributions of 1, 1, and 3.33. The authors are aware of the danger of mixing handling qualities, PIO, and simulator fidelity ratings as suggested in Eq. (1). However, the resulting composite scoring approach was felt to be justified here given that (1) a single-axis task was involved and (2) only the motion system dynamics were varied.

## Pilot/Vehicle Analysis

### Loop Structure

Figure 5 is a block diagram representation of the structural model of the human pilot used in the study. This model forms the assumed pilot compensation in the innermost primary control loop, that is, that loop forming the innermost visual control loop.[2,3] The model was implemented in a MATLAB®-based computer-aided-design package referred to as $\mathrm{PVD_{NL}}$ (Ref. 9). Figure 6 is a block diagram of the complete pilot/vehicle system, with the structural model forming $Y_{P_{\dot h}}$. Thus, an inner, vertical-velocity loop is assumed to serve as the primary control loop. The inner-loop crossover frequency is selected as 2.0 rad/s, as required in the handling qualities assessment technique of Ref. 4. The basis for the loop-closure sequence is that the inner, vertical-velocity loop can be closed with gainlike pilot compensation and that the required visual cue, vertical velocity can be sensed relatively easily by the pilot in the experimental setup.

The outer-loop closure consists of feeding back vertical height error, again a variable that can be easily sensed by the pilot in the experiment. The outer-loop compensation is a simple gain, that is, $Y_{p_h} = K_h$. The separation between the inner- and outer-loop crossover frequencies was selected as a factor of 3. As discussed in Ref. 10, the crossover frequencies in successive loop closures should be separated by a factor of 2–3 in pilot/vehicle analyses. Here, the value of the factor is less important than the fact that it was not varied in the analysis. Thus, the outer height loop is closed at 0.667 rad/s.

### Modeling the Inceptor

The cockpit inceptor that was used in this experiment was the main rotor collective control. The force/feel characteristics of the device are significantly different from a cyclic inceptor or control column in that there are no self-centering characteristics and that there is

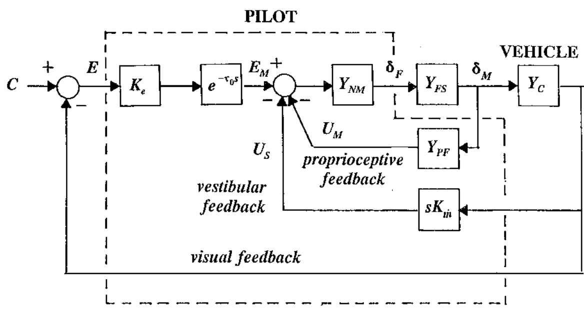


**Fig. 5 Structural Model of the human pilot.**

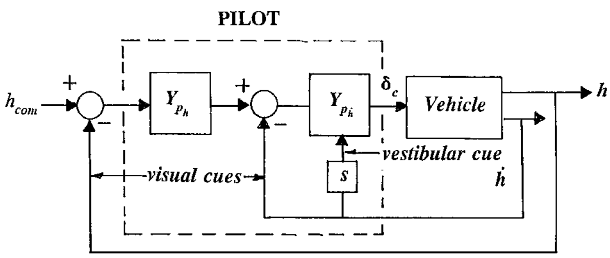


**Fig. 6 Hypothesized pilot/vehicle system for the bob-up/down maneuvers.**

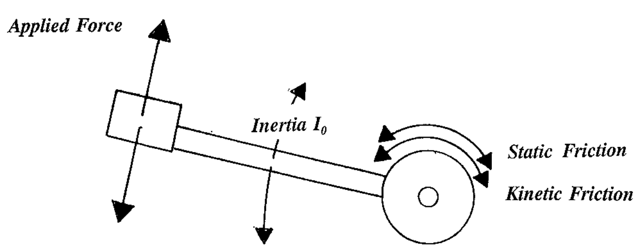


**Fig. 7 Collective inceptor.**

significant and deliberate dry and viscous friction introduced in the device's dynamics as shown in Fig. 7. Because the dynamics of the inceptor are included explicitly in the structural model of Fig. 5, it is important to at least approximate the dynamics of the inceptor. In the absence of a detailed nonlinear model of the collective, an approximate linear model was developed. Space does not permit a detailed description of the development of the linear representation; however, on the basis of a computer simulation of a device with static and kinetic friction as shown in Fig. 7, the following linear model was developed:

$$Y_{\mathrm{FS}} = \frac{1.0}{s(0.1s + 1)} \frac{\text{applied force}}{\text{displacement}} \tag{2}$$

The particular units involved in Eq. (2) are not important here because the gain in the proprioceptive loop of the structural model is selected on the basis of the minimum damping ratio of any quadratic roots of the $\delta_M / E_M$ transfer function of Fig. 5 with all other loops open,[10] regardless of the units involved.

Previous efforts with an earlier version of the structural model have been directed toward modeling the pilot with a variety of inceptors, including those without self-centering characteristics such as the collective control used in this study.[11] It was found that matching measured pilot/vehicle transfer functions with such inceptors required a derivative element to be included in the neuromuscular system model. This derivative element will also be included here. Inclusion of this element is consistent with a human control structure in which inceptor rate is commanded and proprioceptively sensed.

#### Choosing Pilot Model Parameters

References 4 and 9 provide detailed guidelines for choosing the structural model parameters so that the crossover model of the human pilot[12] is in evidence. Pilot model parameter selection is straightforward. Only the results are presented here. Elements $Y_{\mathrm{NM}}$ and $Y_{\mathrm{PF}}$ are given by

$$Y_{\mathrm{NM}} = \frac{\omega_{\mathrm{NM}}^2 s}{s^2 + 2\zeta_{\mathrm{NM}}\omega_{\mathrm{NM}} s + \omega_{\mathrm{NM}}^2} \tag{3}$$

$$Y_{\mathrm{PF}} = K(s + a) \qquad \text{or} \qquad K \qquad \text{or} \qquad K/(s + a) \tag{4}$$

with the particular equalization of Eq. (4) dependent on the form of the vehicle dynamics $Y_c$, in the vicinity of the crossover frequency. The zero at the origin in the neuromuscular system model of Eq. (3) is attributable to the nature of the inceptor, as has just been described. The forms of the last of Eqs. (4) can be interpreted as the pilot's internal model of the vehicle dynamics. That is, in the region of crossover, $Y_{\mathrm{PF}} \propto s \cdot Y_c(s)$. For reasons described in Refs. 4 and 9, a constant crossover frequency $\omega_c = 2.0$ rad/s is chosen.

A number of model parameters are considered invariant across different vehicles and tasks. Nominal values of these fixed parameters can be given as

$$\tau_0 = 0.2 \text{ s} \qquad \omega_{\mathrm{NM}} = 10 \text{ rad/s} \qquad \zeta_{\mathrm{NM}} = 0.7 \tag{5}$$

The relatively simple relations of Eqs. (2–4) and the crossover relation $\omega_c = 2.0$ rad/s are all that are necessary to implement the model of Fig. 5. The selection of one of the three forms on the right-hand side of Eq. (4) is done so that the resulting open-loop transfer function

$$Y_p Y_c = (\delta_M / E)(j\omega) \cdot Y_c(j\omega) \approx (\omega_c / j\omega) e^{-\tau_e s} \qquad \text{for} \qquad \omega \approx \omega_c \tag{6}$$

that is, $Y_p Y_c(j\omega)$ follows the dictates of the crossover model of the human pilot.[12] It is important to specify in a precise manner just how this is done. Limiting discussion to the last two forms of $Y_{\mathrm{PF}}$ (those most likely to be encountered in pilot/vehicle analyses), the right-hand side of Eq. (4) is selected so that

$$\left| \frac{K}{Y_{\mathrm{PF}}(j\omega)} \cdot Y_c(j\omega) \right| \approx \frac{K_1}{j\omega} \qquad \text{for} \qquad \begin{cases} \omega \approx \omega_c \\ K_1 \quad \text{arbitrary} \end{cases} \tag{7}$$

The gain $K$ appearing in Eqs. (4) and (7) is chosen so that, with all other loops open, the minimum damping ratio of any quadratic closed-loop poles of $(\delta_M / E_M)(s)$ is $\zeta_{\min} = 0.15$.

Next, the vestibular loop in Fig. 5 is closed. This loop assumes that the time rate of change of the output of the primary control loop is amenable to sensing by the human vestibular system. The dynamics of a motion system such the washout dynamics of a flight simulator can be included in this loop. The gain $K_{\dot{m}}$ is chosen so that with all other loops open but the proprioceptive loop closed, the minimum damping ratio of any quadratic closed-loop poles of $(\delta_M / E_M)(s)$ is $\zeta_{\min} = 0.05$. Finally, $K_e$ is selected so that the desired crossover frequency of 2.0 rad/s is obtained. The criteria for selecting $K$ and $K_{\dot{m}}$ are based on obtaining an open-loop pilot/vehicle transfer function $(M / E)(s)$ that exhibits, at least in an approximate sense, the high-frequency (10–15 rad/s) characteristics that have been measured in experiment.[10,13]

#### Model Overview

The pilot model of Fig. 5 establishes the framework within which analytical and experimental results will be interpreted. This model has been developed over a number of years and has been used, in one form or another, in a variety of pilot/vehicle analyses. In particular, an earlier version of the model was used to hypothesize the manner in which the human pilot uses vestibular cues.[13] In the study of Ref. 13, it was demonstrated that a model of the human's use of motion cues could be presented that was a simple extension of that for static tracking, that is, with no motion present. In terms of this model, motion does not provide fundamental lead compensation in tracking or regulation tasks, but rather serves to tune the pilot/vehicle dynamics by decreasing high-frequency phase lags occurring in the

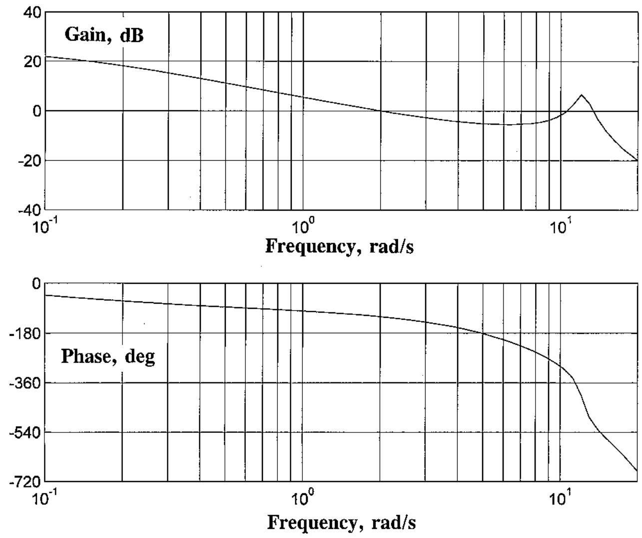


**Fig. 8 Bode diagram of the open-loop pilot/vehicle system for nominal configuration.**

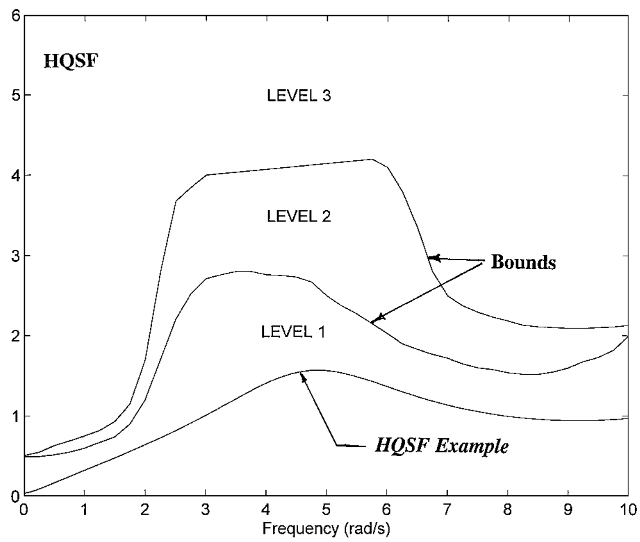


**Fig. 9 HQSF bounds for predicting handling qualities levels.**

effective open-loop pilot/vehicle transfer function after the fundamental pilot compensation is accomplished through the proprioceptive loop closure. Figure 8 is a Bode plot of the pilot/vehicle transfer function $M/E$ from Fig. 5 for the nominal vehicle, showing that the characteristics of the crossover model of the human pilot are in evidence.

#### Handling Qualities Sensitivity Functions

References 4 and 9 provide detailed information on how the structural model can be used to provide predictions of handling qualities. The levels of handling qualities are noted on the Cooper–Harper scale of Fig. 3. Note that, as defined here, level 3 handling qualities extends to a Cooper–Harper rating of 10. The model-based metric that allows prediction of HQR and PIOR levels is the handling qualities sensitivity function (HQSF) defined as

$$\mathrm{HQSF} = (1/K_e)|(U_M/C)(j\omega)| \tag{8}$$

with $K_e$, $U_M$, and $C$ indicated in Fig. 5.

Using flight-test handling qualities results, Ref. 4 demonstrated that the HQSF could be used to discriminate among handling qualities levels 1–3. Figure 9 shows the HQSF bounds that resulted from that study. The predicted handling qualities level for a particular aircraft was determined by the area in Fig. 9 that was penetrated by the HQSF when the pilot model was selected as described earlier. Note that the bounds in Fig. 9 were established using tasks other that a bob-up/down. Indeed, one of the hypotheses of the handling qualities prediction technique discussed in Refs. 4 and 9 is that the bounds should be task independent.

#### Modeling Simulator Limitations

The technique for modeling simulator limitations was to first complete a pilot/vehicle analysis of a nominal vehicle. The nominal vehicle represents the vehicle dynamics representing those of the flight article as closely as possible, that is, not including any of the flight simulator limitations, here limited to variations in motion system characteristics and to time delays associated with the visual and motion system operation. The pilot model parameters thus chosen were then frozen, and the simulator limitations introduced. Changes in the HQSF were then noted and compared with the HQSF of the nominal vehicle. Changes in these functions were then considered evidence of simulation fidelity problems. This technique is a refinement of that proposed in Refs. 2 and 3. It should be emphasized that the resulting handling qualities predictions with simulator limitations are not indicative of those of the vehicle as simulated because no attempt has been made to change the pilot model parameters from those obtained with the nominal vehicle model.

#### Inverse Dynamic Analysis

The pilot/vehicle analysis to be undertaken will involve a computer simulation of the task using the computer-aided-design program of Ref. 9. The pilot/vehicle system of Fig. 6 is compensatory, that is, error signals between command and output variables drive the system. Although such compensatory structures are useful for tracking and regulation tasks, their face validity in the discrete bob-up/down maneuvers such as that being studied here is sometimes called into question. For example, in the past such tasks have been modeled by considering a precognitive rapid-response phase followed by a compensatory error-reduction phase.[14,15] Although such a modeling approach is useful, it complicates the analysis of the maneuver using the handling qualities prediction technique just described. Using the model of Fig. 6 with a 32-ft step input command, however, produces unrealistic tracking results unless nonlinear limiters are introduced at various points in the pilot model. Again, this complicates the analysis, and requires additional assumptions about the saturation values of the limiters. The compensatory structure of Fig. 6 can be retained, however, while still producing realistic results by appealing to inverse dynamic analysis.

The rationale behind using inverse dynamic analysis is that a compensatory structure can still be employed and produce performance comparable to that attained in flight or in pilot-in-the-loop simulation. The problem is approached by posing the following question: Using the compensatory structure of Fig. 6, what command trajectory $h_{\mathrm{com}}(t)$ will produce an $h(t)$ that approximates that obtained in experiment? The answer can be found through inverse dynamic analysis. In the examples to be discussed, a distinction is made between desired and command trajectories. The desired trajectory is the one we wish the vehicle to follow in the task. The command trajectory is one actually employed in the computer simulation of the pilot/vehicle system and that forces the closed-loop compensatory pilot/vehicle system to produce the desired trajectory. Here, the command trajectory was obtained by the expedient of approximating the inverse of the closed-loop pilot/vehicle transfer function over a frequency range extending to approximately 10 rad/s, a range more than adequate for creating an acceptable $h_{\mathrm{com}}$. Thus, the Laplace transform of the command trajectory $[h_{\mathrm{com}}(s)]$ was obtained as

$$h_{\mathrm{com}}(s) = h_{\mathrm{des}}(s) \cdot \{1/[h/h_c(s)]_{\mathrm{approx}}\} \tag{9}$$

where $h_{\mathrm{com}}(s)$ is the command trajectory as just defined, $h_{\mathrm{des}}(s)$ is the desired trajectory as just defined, and $[h/h_c]_{\mathrm{approx}}$ is a proper (as many poles as zeros) approximation to the $h/h_c$ transfer function obtained from the compensatory pilot/vehicle system in Fig. 6, and is valid up to a frequency of 10 rad/s.

In implementing Eq. (9), it was typically necessary to include a pure prediction time, that is, the inverse of a time delay. This prediction time typically was called into play to approximate the phase lag effects of right-half-plane zeros of $h/h_c$ when such zeros were replaced by symmetrical left-half-plane zeros in $[h/h_c]_{\text{approx}}$. Implementing such a predictor in simulation was accomplished by the expedient of eliminating the predictor and simply delaying $h_{\text{des}}(t)$ by an equal amount.

The desired vehicle trajectory was defined here as

$$h_{\text{des}}(t) = \left(\frac{\text{distance}}{16}\right) \cdot \left[\cos\left(\frac{3 \cdot \pi \cdot t}{T_d}\right) - 9 \cdot \cos\left(\frac{\pi \cdot t}{T_d}\right) + 8\right] \text{m} \tag{10}$$

where distance refers to the required vertical translational distance of the bob-up/down maneuvers (32 ft). $T_d$ is the completion time of the maneuver, that is, the first time instant at which $h_{\text{des}}(t) = \text{distance}$. Based on the acceptable time to capture of Ref. 7, $T_d$ was set to 6.5 s.

Of course, no desired trajectory such as that just created was included in the VMS simulation. The pilots were simply asked to meet the performance criteria of Table 2. In the pilot/vehicle analysis, however, the trajectory of Eq. (10) resulted in smooth pilot model inputs with performance meeting the acceptable criteria of Table 2 with the nominal vehicle model.

## Pilot Modeling Results

### Bob-Up Maneuver Time Histories

The pilot modeling results will be presented in terms of a comparison of the HQSF plots for the nominal vehicle and those of the vehicle as simulated in the VMS experiments. Only the bob-up maneuver will be discussed because the modeling results are essentially identical for both bob-up and bob-down. Figures 10–13 show the results of the bob-up maneuver using the program of Ref. 9. Note in Fig. 10 how well the output of the compensatory pilot/vehicle system, $h(t)$, follows the $h_{\text{des}}$ when $h_{\text{com}}$ is applied to the pilot/vehicle system. Figure 13 is of particular interest because it compares the signals $U_M$ (proprioceptive feedback) and $U_S$ (vestibular feedback) in the structural model during the bob-up maneuver. Note that $U_S$ is essentially an attenuated version of $U_M$. This will always be the case in the structural model because $U_M$ will always be proportional to the rate of change of primary control loop output [here $\ddot{h}(t)$] due to pilot control inputs. In an inanimate controller, such redundancy would be unnecessary. In the human controller, however, the vestibular signal may serve as a tuning device for the proprioceptive dynamics $Y_{\text{PF}}$. We will have reason to return to the

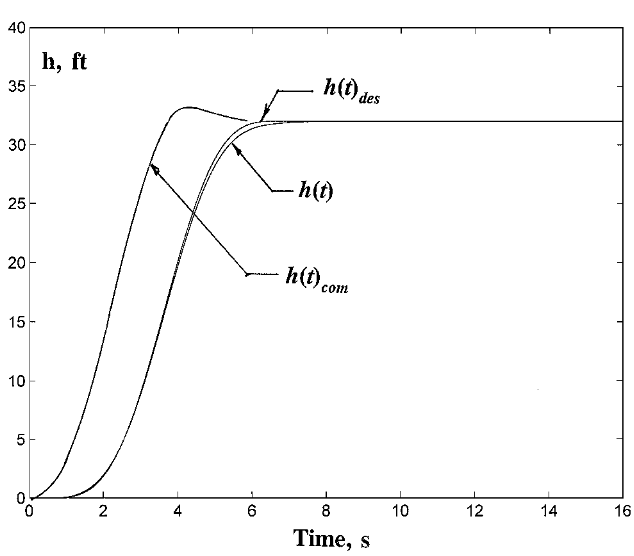


Fig. 10 Height desired, height commanded, and height response of the simulated pilot/vehicle system.

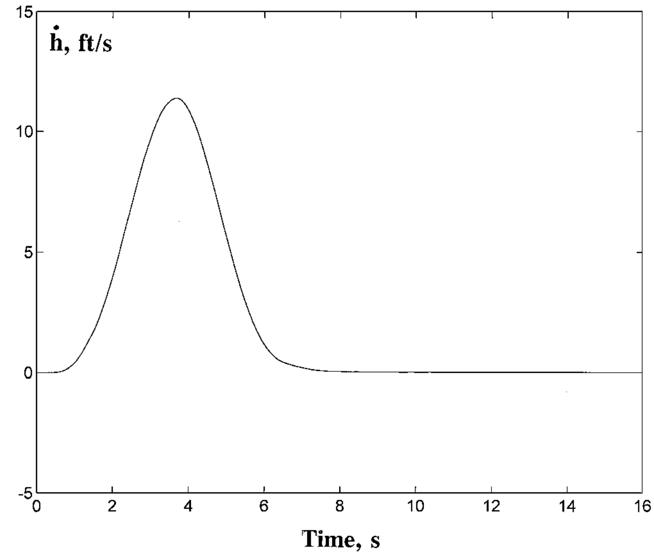


Fig. 11 Vertical-velocity response of the simulated pilot/vehicle system.

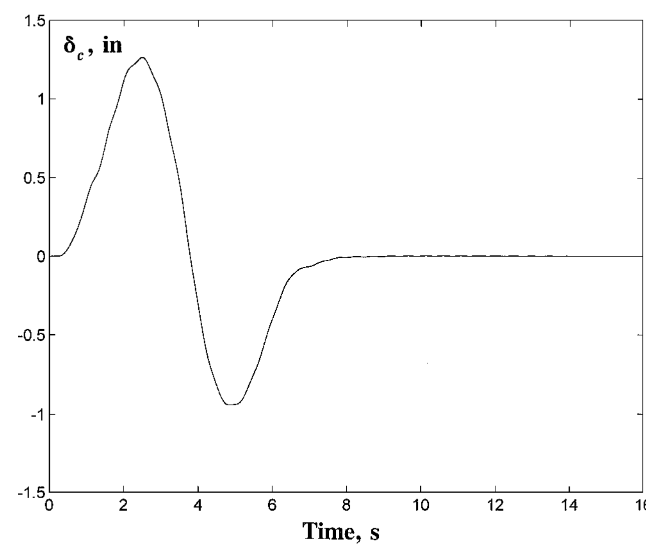


Fig. 12 Collective input in the simulated pilot/vehicle system.

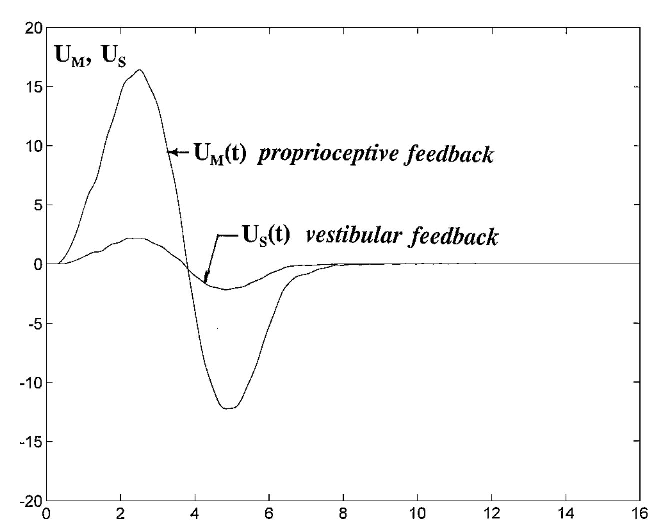


Fig. 13 Proprioceptive and vestibular signals in the simulated pilot/vehicle system.

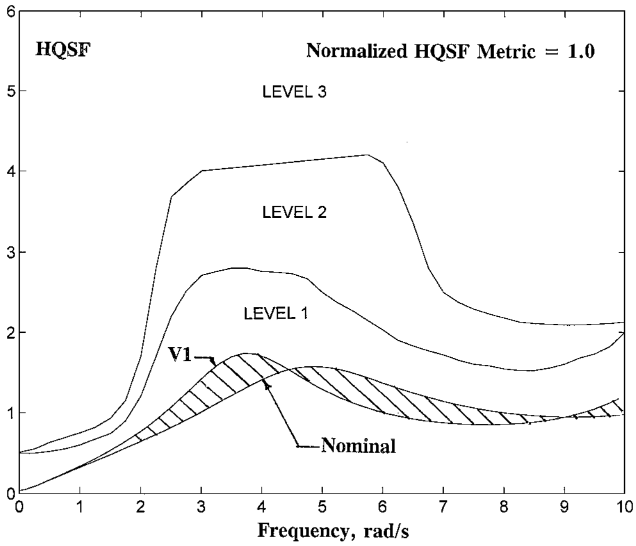


Fig. 14 HQSF comparisons for nominal and V1 configurations.

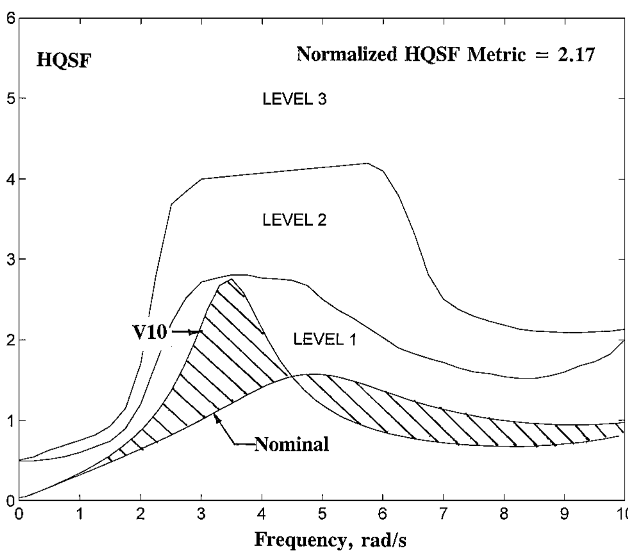


Fig. 15 HQSF comparisons for nominal and V10 configurations.

results of Fig. 13 when the fuzzy-inference identification results are discussed.

### HQSF Comparison

Figures 14–18 show the HQSF for the nominal vehicle compared with that of each of the five motion configurations of Table 1. The shaded areas in Figs. 14–18 indicate the differences between the HQSF for the nominal vehicle and that of the simulated vehicle with simulator motion limitations. A metric based on these area differences was defined as follows and its numerical value is indicated on each of Figs. 14–18:

normalized HQSF metric for configuration $j$

$$= \frac{\int_0^{10} |[\mathrm{HQSF}(\omega)]_j - [\mathrm{HQSF}(\omega)]_{\mathrm{nom}}|\,\mathrm{d}\omega}{\min\limits_{\text{all } j}\left[\int_0^{10} |[\mathrm{HQSF}(\omega)]_j - [\mathrm{HQSF}(\omega)]_{\mathrm{nom}}|\,\mathrm{d}\omega\right]} \tag{11}$$

As in Eq. (1), the denominator of Eq. (11) represents the best system as reflected in the area differences between the HQSFs for the nominal configuration and any of the remaining configurations. The bar graph of Fig. 19 compares these areas with those from the average composite scores of Table 4 and a third metric yet to be described. As can be seen, the order of motion configurations from most like to least like the nominal in terms of area differences between HQSFs

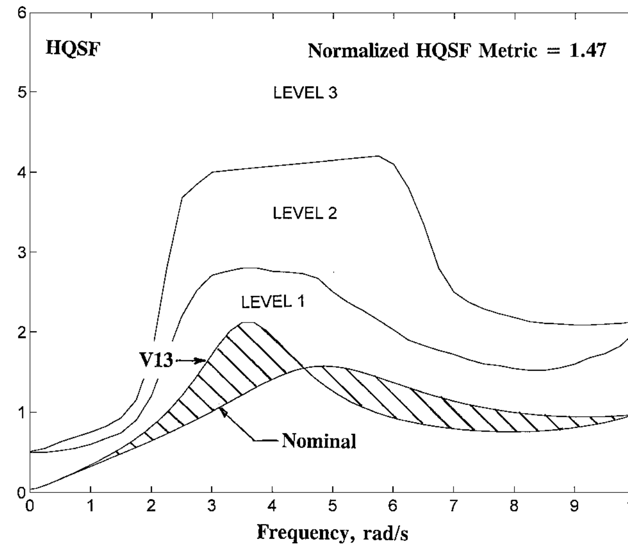


Fig. 16 HQSF comparisons for nominal and V13 configurations.

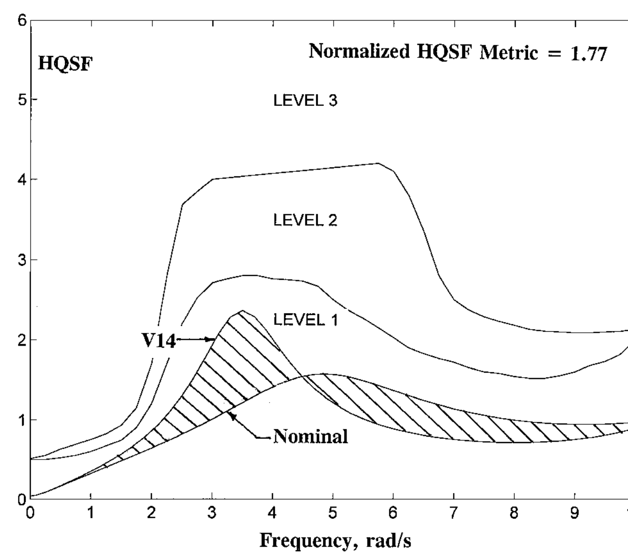


Fig. 17 HQSF comparisons for nominal and V14 configurations.

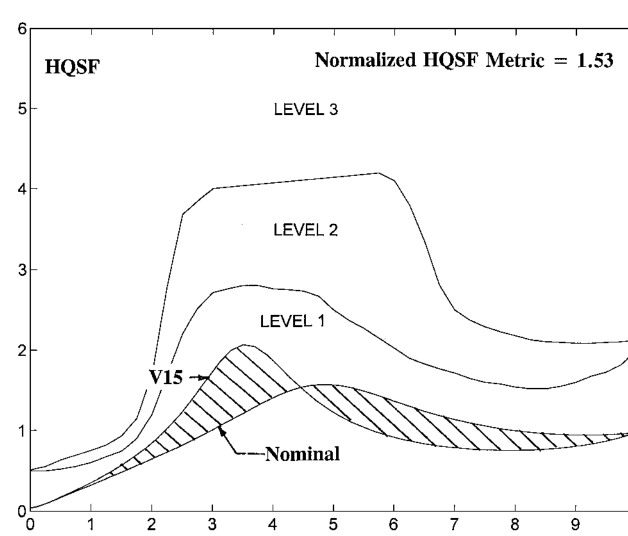


Fig. 18 HQSF comparisons for nominal and V15 configurations.

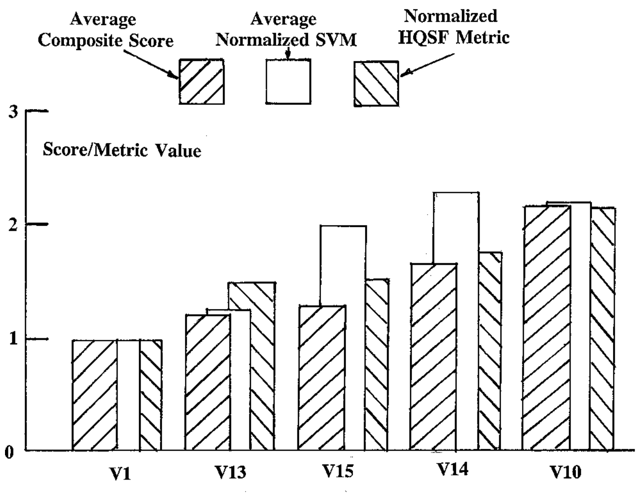


Fig. 19 Bar graph comparison of experimental and analytical results.

are V1, V13, V15, V14, and V10. This ranking is seen to agree with the pilot rating ranking obtained by numerically ordering the average composite scores of Table 4. The caveat here is that there was no nominal configuration in the simulation study, that is, even configuration V1 contained time delays from the visual and motion systems.[7] However, an estimate of the HQRs and PIORs for the nominal vehicle were obtained from the structural model results. These are shown in the last row of Table 4.

## Fuzzy-Inference Identification Results

### Introduction

Fuzzy set theory leads to a description of cause and effect relationships that differ considerably from more classical approaches used to describe dynamic systems.[16] For example, in controlling the height of a rotorcraft in the stabilization mode of a bob-up maneuver, the pilot might define control actions as follows:

1) If the height deviation is large and negative (below the target height) and the vertical velocity is also negative, my collective input is large and positive, that is commanding increased main rotor pitch.

2) If the height deviation is very small and negative and the vertical velocity is small and positive, my collective input is very small and negative.

The if–then type of statements exemplified in the preceding definitions are typical of fuzzy algorithms, as are use of fuzzy-conditional statements such as very small. The fundamental idea in fuzzy systems is a generalization of the concept of a set. In classical set theory, there is a distinct difference between elements that belong to a set and those that do not. Fuzzy set theory allows elements to belong to more than one set, and assigns each element a membership value $M$ between 0 and 1 for each set of which it is a member.

Fuzzy-inference identification (FII) can be thought of as a means of generating membership functions and if–then rules so that the inputs to a dynamic system can be mapped into the output(s) with a high degree of precision, that is, with little matching error. The numerical value of the inputs must be fuzzified to allow application of FII, then defuzzified to allow mapping into the numerical values of the estimated output. This process has been automated in computer-aided design packages such as the MATLAB Fuzzy Logic Toolbox.[17] As will be described, this toolbox was utilized in analyzing the behavior of three of the five pilots participating in the NASA VMS study. The advantages of FII are that no particular structure needs be assumed for the system being identified, no special inputs are required, and nonlinearities pose no particular difficulty. The primary disadvantage of FII, from a control theoretic standpoint, is that the models to which feedback control engineers are most accustomed, for example, transfer functions, are not natural products of FII.

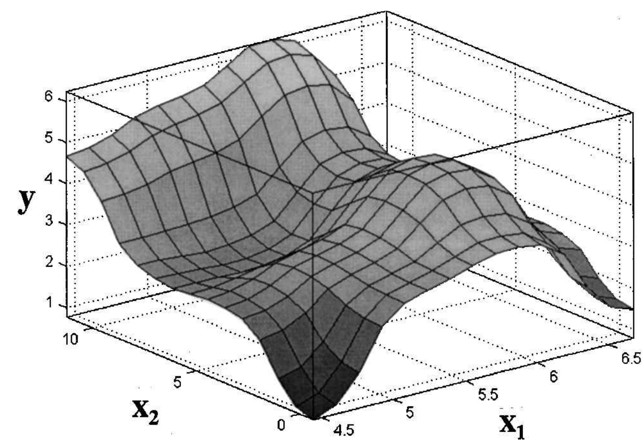


Fig. 20 Surface view plot.

### Interpreting FII Results: Surface View Plot

The if–then rules that result from FII can be interpreted graphically by means of surface view plots. Consider a system to be identified that has two inputs [$x_1(t)$ and $x_2(t)$] and one output [$y(t)$]. Next, set $x_2$ equal to its most negative value obtained in the identification experiment. Then, allow $x_1$ to vary across the range of values encountered in the experiment and allow the if–then rules to trigger, that is, allow them to create the output values. Next, $x_2$ is incremented and the procedure repeated. This process is continued until the most positive $x_2$ value is used. A three-dimensional surface view plot can now be created representing $y = f(x_1, x_2)$, an example of which is shown in Fig. 20. If more than two input variables are in evidence (as will be the case here), surface view plots can still be obtained; however, the remaining input variables are held constant, typically at their average values obtained in the identification experiment. Other constant values, however, can be chosen. Note that the selection of constant values for the variables not explicitly plotted is not equivalent to assuming that they take on such constant values in the FII; rather, this assumption is required for plotting purposes only.

### FII and the Structural Pilot Model

The analytical framework provided by the structural model can also provide some guidance in interpreting the results of FII through surface view plots. In discussing the structural model, it has been hypothesized that the activity in the proprioceptive feedback loop determines the handling qualities level assigned to the vehicle and task. This proprioceptive activity can also be examined in FII through surface view plots. Consider Fig. 5, where now $\delta_M \equiv \delta_c$ and $M \equiv \dot{h}$. Here $\delta_c$ and $\dot{h}$ serve as inputs $x_1$ and $x_2$ with $\delta_c$ also serving as the output $y$, $\delta_c$ is both a pilot input and output, and the surface view is indicating how the variables on the horizontal axes $\delta_c$ and $\dot{h}$ are contributing to the pilot output $\delta_c$ on the vertical axis. If there is no activity in the proprioceptive loop, the resulting surface view plot will be planar and horizontal. In addition, according to the fundamental hypothesis invoked in Ref. 4, the handling qualities will be optimum. This idea is identical to the no tracking hypothesis offered in Ref. 18: "Optimum handling qualities demand minimum closed-loop control by the pilot." As will be seen, one possible experimental measure of the activity in the proprioceptive loop would involve the geometry of the surface view plot just described, that is, how much it deviates from a horizontal planar surface. One measure of this deviation would be the volume beneath the surface view plot, where the volume is measured from a planar horizontal surface containing the lowest point on the surface view plot. Obviously, other choices are possible, for example, the difference between the surface area of the surface view plot and that of a horizontal planar surface with an area equal to that of the vertically projected surface view plot.

### Identification Results

Figure 21 shows the assumed pilot inputs and pilot output for the bob-up/down maneuvers. The appearance of the collective motion

$\delta_c$ as both an input and output variable reflects the role of that variable as a pilot output and as a hypothesized feedback quantity in the proprioceptive loop of the pilot model of Fig. 5. At this juncture a question may arise as to why the FII does not simply ignore all input variables save $\delta_c$ and then produce a one-to-one mapping between the $\delta_c$ input and the $\delta_c$ output. The answer is that FII assumes that all of the inputs specified by the user affect the output. The FII algorithm adjusts the membership functions and fuzzy rules to optimize the mapping of this prescribed input–output set. Figure 22 is a sample comparison of the collective time history from one of the bob-up maneuvers and the FII that resulted. The FII output is obtained by using the assumed pilot inputs shown in Fig. 21 as inputs to the identified fuzzy model of the pilot. The training parameter optimization for the FII was based on the Sugeno–Takagi–Kant model that implies that the output is a linear combination of the inputs.[17] Four triangular membership functions were assigned for each input, resulting in 256 ($4^4$) rules being generated as part of the fuzzy logic. The FII training was performed until the root-mean square error between model and pilot (VMS simulator) output was less than $1 \times 10^{-5}$ in. All of the FII results were of the quality shown in Fig. 22. As an example of the nature of the surface view plots, Fig. 23 shows results for a single bob-up and bob-down maneuver for pilot A for configuration V1.

Because three repetitions of the two separate maneuvers (bob-up and bob-down) were utilized in the experiment, some means of averaging these was necessary to obtain a single metric for comparison with handling qualities, etc. The following average normalized surface view metric (SVM) was created:

average normal SVM, configuration $j$

$$= \sum_{i=1}^{3}\left[\sum_{k=1}^{3}\left(V_{\mathrm{BU}_k}\right)_j + \sum_{k=1}^{3}\left(V_{\mathrm{BD}_k}\right)_j\right] \Bigg/ \min_{\text{all } i \,\&\, \text{all } j}\left\{\sum_{i=1}^{3}\left[\sum_{k=1}^{3}\left(V_{\mathrm{BU}_k}\right)_j + \sum_{k=1}^{3}\left(V_{\mathrm{BD}_k}\right)_j\right]\right\} \tag{12}$$

where $i$ represents results for the $i$th pilot, $V_{\mathrm{BU}_k}$ is the volume above minimum vertical coordinate on the surface view plot for the $k$th bob-up, $V_{\mathrm{BD}_k}$ is the volume above the minimum vertical coordinate on the surface view plot for the $k$th bob-down, and $\min_{\text{all } i\&j}$ is the minimum sum of the volumes for all pilots and configurations. In the bob-down maneuver, the collective, vertical-velocity and vertical-acceleration signals were modified so that the surface view plots could be more easily compared to those in the bob-up maneuver. For the bob-down maneuver, these modifications were

$$(\text{vertical acceleration})_{\text{mod}} = -(\text{vertical acceleration}) - 64\ \text{ft/s}^2$$

$$(\text{collective})_{\text{mod}} = 11 - \text{collective in.}$$

$$(\text{vertical velocity})_{\text{down}} = -(\text{vertical velocity})\ \text{ft/s} \tag{13}$$

Also, the remaining input variables not included on the surface view plot, that is, height error and vertical acceleration (for all but configuration V10) were set to values representing the terminal part of the maneuver.

The last column of Table 4 represents the average normalized SVM calculated as given in Eq. (12). The bar graph of Fig. 19 compares the average normalized SVM and the average composite scores. The order of the motion configurations from most like to

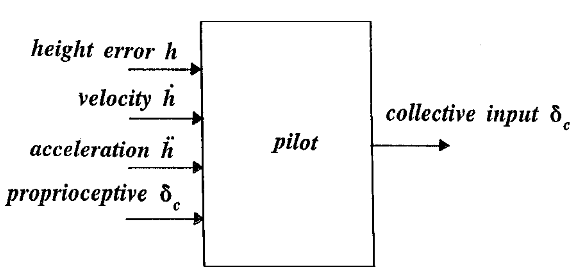


**Fig. 21 Hypothesized pilot inputs and output for FII in the bob-up/down maneuvers.**

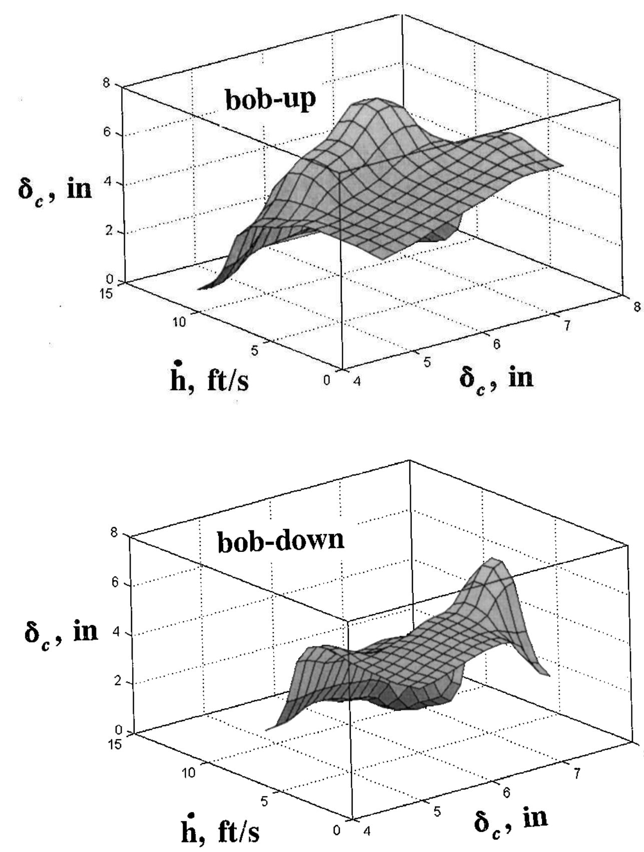


**Fig. 23 Surface view plots for bob-up and bob-down maneuver: pilot A, and configuration V1.**

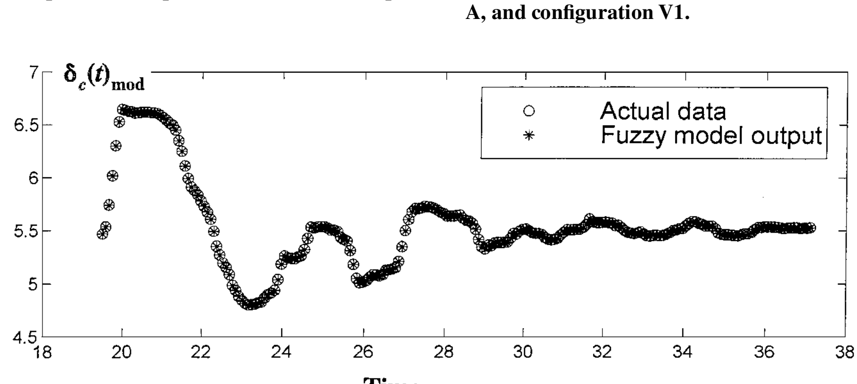


**Fig. 22 Example of FII: comparing collective time histories from experiment and identified fuzzy pilot model.**

least like the nominal is seen to be V1, V13, V15, V14, and V10. One sees that the ordering of the last two configurations differs from that established with the average composite scores. Nonetheless, the results are noteworthy. Metrics other than Eq. (12) can be employed, of course. The metric of Eq. (12) was chosen because of its relation to activity in the assumed primary control loop in the bob-up/down maneuvers. Obviously more research in this area is warranted.

## Discussion

One important hypothesis regarding pilot utilization of proprioceptive and vestibular cues can be advanced based on the research described herein, namely, that in a control-theoretic sense both the vestibular and proprioceptive feedback signals provide redundant information. However, the vestibular feedback may be of higher quality, with a broader bandwidth than that obtainable from proprioceptors. In this light, the vestibular feedback may serve to tune the dynamics of the proprioceptive feedback loop in addition to decreasing phase lags in the transfer function of the open-loop pilot/vehicle system. When the quality of the vestibular information is degraded from nominal, the FII clearly shows an increase in proprioceptive activity that also has been hypothesized to be a harbinger of degraded handling qualities.[4] Degradations in handling qualities were indeed noted in the pilot ratings from the simulation experiment when the motion system characteristics were degraded through either gain reduction or washout dynamics.

The results presented have been limited to a single-axis control task. Extension of the results to multiaxis tasks is an obvious prerequisite to the practical evaluation of simulator fidelity. Research is continuing in this area.

Finally, the authors are aware that somewhat specialized software is needed in application of the analysis and identification techniques that have been described. The MATLAB- based pilot model program described in Ref. 9 is available from the second author, and the fuzzy-inference software is commercially available.

## Conclusions

An analytical and experimental investigation of the manner in which pilots perceive and utilize visual, proprioceptive, and vestibular cues in a ground-based flight simulator led to the development of a pair of metrics that were used to assess simulator fidelity.

1) The analytical approach used an established pilot/vehicle analysis technique based on a structural model of the pilot from which were obtained HQSFs. A metric based on area differences between the sensitivity functions for the nominal and simulated pilot/vehicle system was shown to correlate well with composite rating scores obtained from a simulation experiment conducted on the NASA Ames Research Center VMS.

2) FII was exercised using the NASA simulation data for three pilots. A total of 90 separate identifications were completed. After identifying the fuzzy pilot models for each pilot, surface view plots were obtained that graphically displayed the results of the identification. A metric based on the geometry of these plots was also shown to correlate well with the composite rating scores obtained from the experiment.

3) Further research is warranted in extending this methodology to multi axis tasks and in refining the fidelity metric used in the FII results.

## Acknowledgments

The research described has been supported under a NASA Ames Research Center–University of California, Davis Joint Research Interchange NCC2-5238. The NASA researchers responsible for the design and conduct of the simulation experiment are William Chung (now with Logicon-Syre Corporation), Duc Tran, and Jefferey Schroeder.

## References

[1] Atencio, A., Jr., "Fidelity Assessment of a UH-60A Simulation on the NASA Ames Vertical Motion Simulator," NASA TM 104016, 1993.

[2] Hess, R. A., and Malsbury, T., "Closed-Loop Assessment of Flight Simulator Fidelity," *Journal of Guidance, Control and Dynamics*, Vol. 14, No. 1, 1991, pp. 191–197.

[3] Hess, R. A., Malsbury, T., and Atencio, A., Jr., "Flight Simulator Fidelity Assessment in a Rotorcraft Lateral Translation Maneuver," *Journal of Guidance, Control, and Dynamics*, Vol. 16, No. 1, 1993, pp. 79–85.

[4] Hess, R. A., "Unified Theory for Aircraft Handling Qualities and Adverse Aircraft-Pilot Coupling," *Journal of Guidance, Control, and Dynamics*, Vol. 20, No. 6, 1997, pp. 1141–1148.

[5] Kramer, U., and Rohr, G., "A Model of Driver Behavior," *Ergonomics*, Vol. 25, No. 10, 1982, pp. 891–907.

[6] Wu, J. C., and Liu, T. S., "A Fuzzy Model of Rider Control for a Motorcycle Undergoing Lane Change," *International Journal of Vehicle Design*, Vol. 15, Nos. 1/2, 1994, pp. 27–44.

[7] Schroeder, J. A., Chung, W. W. Y., and Hess, R. A., "Spatial Frequency and Platform Motion Effects on Helicopter Altitude Control," AIAA Paper 99-4113, 1999.

[8] Powers, B., "Space Shuttle Pilot-Induced-Oscillation Research Testing," AGARDograph 262, 1984.

[9] Zeyada, Y., and Hess, R. A., "$PVD_{NL}$, Pilot/Vehicle $Dynamics_{NonLinear}$, An Interactive Computer Program for Modeling the Human Pilot in Single-Axis Linear and Nonlinear Tracking Tasks," Dept. of Mechanical and Aeronautical Engineering, Univ. of California, Davis, CA, 1998.

[10] Hess, R. A., "Feedback Control Models—Manual Control and Tracking," *Handbook of Human Factors and Ergonomics*, 2nd ed., edited by G. Salvendy, Wiley, New York, 1997, Chap. 38.

[11] Hess, R. A., "Analyzing Manipulator and Feel System Effects in Aircraft Flight Control," *IEEE Transactions on Systems, Man, and Cybernetics*, Vol. 20, No. 4, 1990, pp. 923–931.

[12] McRuer, D. T., and Krendel, E., "Mathematical Models of Human Pilot Behavior," AGARDograph 188, 1974.

[13] Hess, R. A., "Model for Human Use of Motion Cues in Vehicular Control," *Journal of Guidance, Control, and Dynamics*, Vol. 13, No. 3, 1990, pp. 476–482.

[14] Ferguson, S. W., Clement, W. F., Cleveland, W. B., and Key, D. L., "Assessment of Simulation Fidelity Using Measurements of Piloting Technique in Flight," American Helicopter Society, Paper A-84-40-08-4000, May 1984.

[15] Ferguson, S. W., Clement, W. F., Hoh, R. H., and Cleveland, W. B., "Assessment of Simulation Fidelity Using Measurements of Piloting Technique in Flight, Part II," American Helicopter Society, 41st Annual American Helicopter Society Forum, May 1985.

[16] Zadeh, L. A., "Outline of a New Approach to the Analysis of Complex Systems and Decision Processes," *IEEE Transactions on Systems, Man, and Cybernetics*, Vol. SMC-3, No. 11, 1973, pp. 28–44.

[17] Fuzzy Logic Toolbox for Use with MATLAB, User's Guide, MathWorks, Natick, MA, 1998.

[18] Smith, R. E., and Geddes, N., "Handling Qualities Requirements for Advanced Aircraft Design: Longitudinal Mode," U.S. Air Force Flight Dynamics Lab., AFFDL-TR-78-154, Wright–Patterson AFB, OH, Aug. 1979.